DeepMTL Pro: Deep Learning Based Multiple Transmitter Localization and Power Estimation

Caitao Zhan [a],*, Mohammad Ghaderibaneh [a], Pranjal Sahu [b], Himanshu Gupta [a]

[a] *Stony Brook University, 100 Nicolls Rd, Stony Brook, NY, 11794, USA*
[b] *Kitware, 101 E Eeaver St, Carrboro, NC, 27510, USA*

ARTICLE INFO

ABSTRACT

In this paper, we address the problem of Multiple Transmitter Localization (MTL). MTL is to determine the locations of potential multiple transmitters in a field, based on readings from a distributed set of sensors. In contrast to the widely studied single transmitter localization problem, the MTL problem has only been studied recently in a few works. MTL is of great significance in many applications wherein intruders may be present. E.g., in shared spectrum systems, detection of unauthorized transmitters and estimating their power are imperative to efficient utilization of the shared spectrum.

In this paper, we present DeepMTL, a novel deep learning approach to address the MTL problem. In particular, we frame MTL as a sequence of two steps, each of which is a computer vision problem: image-to-image translation and object detection. The first step of image-to-image translation essentially maps an input image representing sensor readings to an image representing the distribution of transmitter locations, and the second object detection step derives precise locations of transmitters from the image of transmitter distributions. For the first step, we design our learning model sen2peak, while for the second step, we customize a state-of-the-art object detection model YOLOv3-cust. Using DeepMTL as a building block, we also develop techniques to estimate transmit power of the localized transmitters. We demonstrate the effectiveness of our approach via extensive large-scale simulations and show that our approach outperforms the previous approaches significantly (by 50% or more) in performance metrics including localization error, miss rate, and false alarm rate. Our method also incurs a very small latency. We evaluate our techniques over a small-scale area with real testbed data and the testbed results align with the simulation results.

© 2022 Elsevier B.V. All rights reserved.

1. Introduction

The RF spectrum is a limited natural resource in great demand due to the unabated increase in mobile (and hence, wireless) data consumption [1,2]. In 2020, the U.S. FCC moves to free up 100 MHz of previously military occupied mid-band spectrum in the 3.45–3.55 GHz band for paving the way for 5G development. Also, the research and industry communities have been addressing this capacity crunch via the development of *shared spectrum*. Spectrum sharing is the simultaneous usage of a specific frequency band in a specific geographical area and time by a number of independent entities where harmful electromagnetic interference is mitigated through agreement (i.e., policy, protocol) [3]. Spectrum

---

* Corresponding author.
 E-mail addresses: cbzhan@cs.stonybrook.edu (C. Zhan), mghaderibane@cs.stonybrook.edu (M. Ghaderibaneh), pranjal.sahu@kitware.com (P. Sahu), hgupta@cs.stonybrook.edu (H. Gupta).
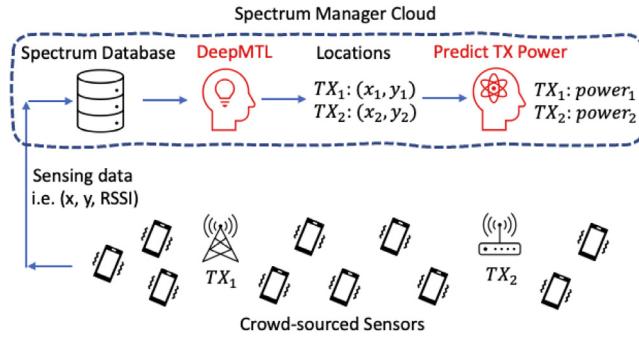
Fig. 1. Multiple transmitter localization using a distributed set of sensors. Sensing data is uploaded to a spectrum manager server in the cloud. DeepMTL is a deep learning approach to multiple transmitter localization which helps protect spectrum against unauthorized usage. After that, prediction of transmission powers happens using DeepMTL as a building block.

sharing techniques are also normally used in 5G networks to enhance spectrum efficiency [4]. However, protection of spectrum from unauthorized users is important in maximizing spectrum utilization.

The increasing affordability of the software-defined radio (SDR) technologies makes the shared spectrum particularly prone to unauthorized usage or security attacks. With easy access to SDR devices (e.g. HackRF, USRP), it is easy for selfish users to transmit data on a shared spectrum without any authorization and potentially causing harmful interference to the incumbent users. Such illegal spectrum usage could also happen as a result of infiltration of computer viruses or malware on SDR devices. [4] depicts three cases of spectrum attack. As the fundamental objective behind such shared spectrum paradigms is to maximize spectrum utilization, the viability of such systems depends on the ability to effectively guard the shared spectrum against unauthorized usage. The current mechanisms however to locate such unauthorized users (intruders) are human-intensive and time-consuming, involving the FCC enforcement bureau which detects violations via complaints and manual investigation [5]. Motivated by the above, we seek an effective technique that is able to accurately localize multiple simultaneous intruders (transmitters). Below, we describe the multiple transmitter localization problem.

Multiple Transmitter Localization (MTL). The transmitter localization problem has been well studied, but most of the focus has been on localizing a *single* transmitter at a time. However, it is important to localize multiple transmitters simultaneously to effectively guard a shared spectrum system. E.g., a malware or virus-based attachment could simultaneously cause many devices to violate spectrum allocation rules; spectrum jamming attacks would typically involve multiple transmitters. More importantly, a technique limited by the localization of a single intruder could then be easily circumvented by an offender by using multiple devices. The key challenge in solving the multiple transmitter localization (MTL) problem comes from the fact that the deployed sensor would receive only a *sum* of the signals from multiple transmitters, and separating the signals may be impossible.

Prior Works. The MTL problem has been recently addressed in a few prior works, among which SPLOT [5], MAP* [6], and DeepTxFinder [7] are the most prominent. SPLOT essentially decomposes the MTL problem to multiple single-transmitter localization problems based on the sensors with the highest power readings in a neighborhood. However, their technique implicitly assumes a propagation model, and thus, may not work effectively in areas with complex propagation characteristics, and it is not effective in the case of transmitters being located close by (a key challenging scenario for MTL problem). Our recent work MAP* solves the MTL problem using a hypothesis-driven Bayesian approach; in particular, it uses prior training in the form of distributions of sensor readings for various transmitter locations, and uses the training data to determine the most likely configuration (i.e., transmitters' locations and powers) for a given vector of sensor readings. However, to circumvent the high computational cost of a pure Bayesian approach, MAP* uses a divide and conquer heuristic which results in somewhat high number of misses and false alarms while still incurring high latency. DeepTxFinder uses a CNN-based learning model approach; however, they use a separate CNN model for a specific number of transmitters and thus may incur high model complexity and training cost while also limiting the number of transmitters that can be localized. In our evaluations, we compare our work with each of the above approaches.

DeepMTL: Our Two-Step Approach. As in prior works [5,8], we assume a crowdsourced sensing architecture (See Fig. 1) wherein relatively low-cost spectrum sensors are available for gathering signal strength in the form of received power. We use a convolutional neural network (CNN) based approach to solve the MTL problem. In particular, we frame MTL as a sequence of two steps: image-to-image translation and object detection, each of which is solved using a trained CNN model. The first step of image-to-image translation maps an input image representing sensor readings to an image representing the distribution of transmitter locations, and the second object detection step derives precise locations of transmitters from the image of transmitter distributions. We name our MTL approach as DeepMTL.

Motivation. Our overall approach and its various aspects are motivated by the following considerations. **First**, we use a learning-based strategy to preclude assuming a propagation model [5] or conducting surveys of sensors reading

distributions [6]. Assumption of propagation model suffers from the fact that even sophisticated propagation models yield unsatisfactory accuracy and thus lead to degraded performance. Among all learning-based strategies, deep learning can implicitly capture the environment characteristics (e.g., objects, walls, landscape) in the neural network layers' weights learned through the training of the data [9]. Even though a learning-based approach incurs a one-time high training cost, it generally incurs minimal latency during inference, which is an important consideration for our MTL problem. The intruder detection should incur minimal latency to be effective. **Second**, the geographical nature of the MTL problem suggests that convolutional neural networks (CNNs) are well-suited for efficient learning of the desired function. In particular, the features of the MTL problem can be represented in an image (2D matrix) corresponding to their geographic locations, which can be fed as an input to an appropriate CNN model which can leverage the spatial correlation among the input features to facilitate efficient learning. **Lastly,** we use a two-step architecture to facilitate efficient training by essentially providing an additional intermediate image. In particular, we are able to map each step to well-studied standard computer vision problems, allowing us to build upon known techniques.

Overall Contributions. The goal of our work is to develop an efficient technique for accurate localization of simultaneously present multiple transmitters/intruders. We also extend our technique to address various extensions such as power estimation and the presence of authorized users. Overall, we make the following contributions.

1. For the MTL problem, we develop a novel two-step CNN-based approach called DeepMTL approach. For the first step of image-to-image translation, we develop a CNN model that translates an image representing the sensor readings into an intermediate image that encodes distributions of transmitter locations (Section 3). For the second step of mapping transmitter distributions to precision locations via object detection, we customize the well-known object detection method YOLOv3 (Section 4).
2. For localization of transmitters in presence of authorized users, we augment the DeepMTL model by adding a pre-processing step based on a CNN-model that first reduces the sensor readings by the power received from the authorized users (Section 5).
3. To estimate transmit power of the intruders, we augment our DeepMTL model with a power-estimation CNN-model which iteratively estimates the power of transmitters in sub-areas (Section 6).
4. We evaluate our techniques via large-scale simulations as well as a small-scale testbed data and demonstrate their effectiveness and superior performance compared to the prior works (Section 7).

A preliminary version of this paper appeared at IEEE WoWMoM 2021 [10].

2. Background, MTL problem and our approach

In this section, we describe the background of the shared spectrum systems, formulate the MTL problem, then describe our methodology.

Shared Spectrum System. In a shared spectrum paradigm, the spectrum is shared among licensed users (primary users, PUs) and unlicensed users (secondary users, SUs) in such a way that the transmission from secondaries does not interfere with that of the primaries (or secondaries from a higher-tier, in case of a multi-tier shared spectrum system). In some shared spectrum systems, the location and transmit power of the primary users may be unavailable, as is the case with military or navy radars in the CBRS band. Such sharing of spectrum is generally orchestrated by a centralized entity called *spectrum manager*, such as a spectrum database in TV white space [11] or a central spectrum access system in the CBRS 3.5 GHz shared band [12]. The spectrum manager allocates spectrum to requesting secondaries (i.e., permission to transmit up to a certain transmit power at their location) appropriately so as to avoid interference to primaries. Users that transmit without explicit permission are referred to as unauthorized users or *intruders*; the MTL problem is to essentially localize such intruders.

MTL Problem. Consider a geographic area with a shared spectrum. Without loss of generality, we assume a single wireless frequency[1] throughout this paper.[2] For localization of intruders, we assume available crowdsourced sensors that can observe received signal in the wireless frequency of interest, and compute (total) received signal strength (RSS). RSS can be measured using low-cost sensors and has been shown to achieve good accuracy for single-transmitter localization [13]. In the related work Section 8, we will discuss signal metrics other than RSS, such as AoA, ToA, etc. At any instant, there may be a set of intruders present in the area with each intruder at a certain location transmitting with a certain power which may be different for different intruders.

The MTL problem is to determine the set of intruders with their locations at each instant of time, based on the set of sensor observations at that instant. For the main MTL problem, we assume that there are no primary or authorized users, and thus, assume that the sensor readings represent aggregate received power from the transmitters we wish to localize. However, in Section 5, we investigate the more general MTL problem where the background primary and/or secondary users may also be present.

---

[1] To avoid confusion with image channels, we use *wireless frequency* instead of the perhaps more appropriate *wireless channel* term.

[2] Multiple wireless frequencies can be handled independently. Note that if we assume the wireless propagation characteristics to be similar for different frequencies, then we do not need to train different models for each of them. Our localization techniques would still work for scenarios wherein the intruders may change their transmit frequencies dynamically.
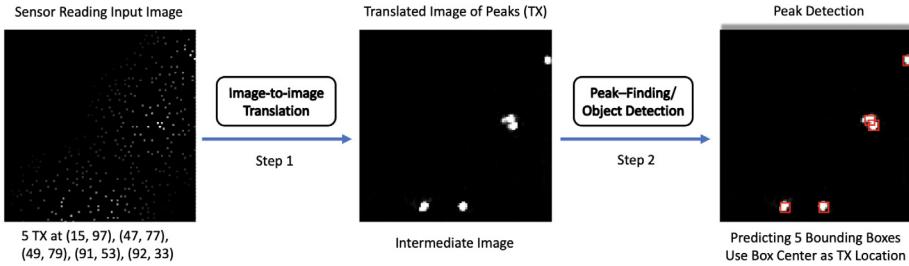
Fig. 2. The overall two-step CNN architecture of the `DeepMTL` model. The first step is the `sen2peak`, whose higher idea is to translate the input image of sensor readings to the image of peaks where each peak implies a transmitter. The `sen2peak` architecture is illustrated in Fig. 4. The second step is `YOLOv3-cust`, a customized version of YOLOv3, to perform object/peak detection in the output image of the first step. This step returns the precise location coordinates of TX. The `YOLOv3-cust` architecture is illustrated in Fig. 5. A zoom-in of the peak detection result of the second step is in Fig. 6.

Our Approach. In our context, each sensor communicates its observation to a centralized spectrum manager which then runs localization algorithms to localize any potential (multiple) transmitters. We design and implement a novel two-step localization algorithm named `DeepMTL`, as illustrated in Fig. 2, based on CNN models. The first step (Section 3) is a four-layer image-to-image translation CNN model that is trained to translate an input image representing sensor readings to an image of transmitters' locations distributions. Each distribution of a transmitter can be visualized as a mountain with a peak, so we name this model `sen2peak`. The second step (Section 4), called `YOLOv3-cust`, is a customized object-detection method build upon YOLOv3 [14] which localize the objects/peaks in the translated image. The high-level motivation behind our two-step design is to frame the overall `MTL` problem in terms of well-studied learning problem(s). The two steps facilitate efficient learning of the models by supplying an intermediate image with the training samples.

3. `DeepMTL` step 1: Sensor readings to TX location distributions

In this section, we present the first step of our overall approach to the `MTL` problem, i.e., the image-to-image translation step which translates/transforms the sensor reading to distributions of TX locations. Here, we first create a grayscale image to represent the input sensor readings; this image encodes both the sensors' RSS readings and the sensors' physical location. We then train and use a convolutional neural network (CNN) model to transform this input image to an output image which represents the distribution of TX locations. Pixels in the output image that have higher values will have a higher chance of having a TX being present at that location.

Input/Output Image Sizes and Tiling Approach for Large Areas. We need to represent data by images of certain sizes. Typically, an image should be a size of a few hundred pixels by a few hundred pixels, since a thousand pixels by thousand pixels images will consume too much GPU memory. In this paper, we pick 100×100 as the size for both our input and output images in the first image-to-image translation step. Given an area that we want to monitor and a 100×100 size image, we will know how large an area a pixel will represent and we call it a pixel subarea. A large pixel subarea could certainly lead to high localization errors, due to very coarse granularity. We can address this by using a "tiling" technique, wherein we divide the given area into tiles, then represent each tile by 100×100 size image and use our localization techniques in the tile. We can do some post-processing to handle cross-tiling issues (e.g., [7] uses overlapping tiles and employs a voting scheme inside the overlapping tile area).

3.1. Input image representing sensors' readings

We localize transmitters based on observations from a set of sensors, i.e. solve the `MTL` problem assuming only intruders. The input of the localization method is sensor observations. Here, an *observation* at a sensor is the received power (RSS, in decibels) over a time window of a certain duration, in the frequency of interest (we assume only one wireless frequency). RSS is computed using FFT over the I/Q samples collected in a time window. More specifically, in our evaluations, we use a Python API [15] that computes the power spectral density from a sequence of signal data (I/Q samples), and then, we choose the RSS at the frequency of interest. Different than [5,6], we represent the sensor information, i.e., their locations and observations, in a 2D input image. We use a 2D grayscale image, and let us denote it $\mathbf{X}$. The pixel $\mathbf{X_{i,j}}$ denotes the observation of the sensor at the grid cell whose index is (i, j). For example, $\mathbf{X}_{10,20} = -50$ denotes there is a sensor at coordinate $(10, 20)$ with an RSS reading of -50 dB. If there is no sensor at location (i, j), we assign the noise floor $\mathcal{N}$ (i.e. -80 dB) value to $\mathbf{X_{i,j}}$. Note that the above pixel values (representing the sensor observations) are not the standard image pixel values that lie in the [0, 255] range. Also, since the pathloss computed by propagation models during simulations could be real numbers, the sensor observation values could be real numbers. So we use a 2D matrix with real numbers instead of an image object.
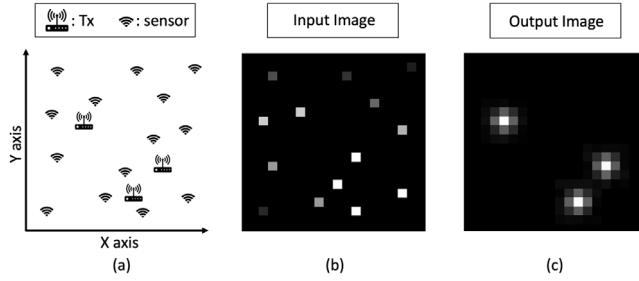
Fig. 3. Illustration of DeepMTL first step's input and output images. (a) Area with distributed sensors and transmitters to be localized. (b) Input image representing the sensor readings (RSS) and locations. (c) Output Image, where we put a 2D Gaussian distribution with its "peak" at the transmitter's location.

Before passing this sensor reading image as input to our CNN model, we do a normalization step; we first subtract the $\mathcal{N}$ from each value and then divide it by $-\mathcal{N}/2$. Let $\mathbf{X}'$ denote the 2D matrix after the normalization of $\mathbf{X}$. The value $\mathbf{X}'_{i,j}$ will be zero at locations without sensors, and $\mathbf{X}'_{i,j}$ will be a positive real number (in most cases, less than two) for locations with sensors. E.g., if $\mathbf{X}_{10,20} = -50$, then the $\mathbf{X}'_{10,20}$ equals to $(-50 - (-80))/40 = 0.75$. Fig. 3(b) shows how a matrix is used to represent the input information that contains both the RSS and the spatial location of the distributed sensors in an area that exists 14 sensors in Fig. 3(a).

3.2. Output image representing TX locations' distributions

We now focus on designing the output image to represent the distribution of TX locations; the output image is essentially the "label" assigned to each input image that guides the training of the CNN model. Fig. 3(c) illustrates the output image of the image-to-image translation step in Fig. 3(a) that contains three transmitters.

A straightforward representation that represents the TXs with locations is to just use an array of (x, y) elements where each (x, y) element is the location of a transmitter, as in [7]. However, this simple representation is less conducive to efficient model learning, as the representation moves away from spatial representation (by representing locations as positions in the image) to direct representation of locations by coordinate values. E.g., in [7]'s CNN-based approach to MTL problem, the authors assume a maximum number N of transmitters and train as many as $N + 2$ different CNN models and thus, limiting the overall solution to the pre-defined maximum number of transmitters. Instead, in our approach, we facilitate the learning of the overall model, by solving the MTL problem in two steps, and in this step of translating sensors' reading to transmitter locations' distributions, we represent the output also as an image. This approach allows us to use a spatial learning model (e.g. CNN) for the second step too, and preclude use of regression or fully-connected layers in the first step.

Inspired by recent work on wireless localization problem [9] that represents the input and output as images, we represent our output of the first step as an image as well. The output image is a grayscale image implemented as a 2D matrix with real numbers. In the output image, we use 25 (5×5) pixel values to represent the presence of a transmitter. It is desirable to use an odd side length square (e.g., $3 \times 3, 5 \times 5, 7 \times 7$) for symmetry. For a 100×100 size input we use, while 3×3 gives too little information for a transmitter and 7×7 generates too many overlaps for close by transmitters, 5×5 is the sweet spot. Other pixels far away from any transmitter are zero-valued. Among multiple potential ways to represent a transmitter presence by a number of pixels, we found that using a 2D Gaussian distribution around the pixel of TX location, as shown in Fig. 3(c), yields the best model performance. Thus, a geographic area with multiple transmitters present is represented by a grayscale image with multiple Gaussian distributions, with each Gaussian distribution's peak inside the pixel corresponding to transmitter's location. Based on preliminary performance tests, we pick the amplitude of the 2D Gaussian peak to 10, the standard deviation to 0.9, and located the center of the distribution at the location of each transmitter. Note that the location of the TX is in continuous domain and usually not at the center of the grid cell.

3.3. Image-to-image translation: sen2peak CNN model

At a higher level, we use a deep and spatial neural network, in particular a CNN, to learn the approximation function that maps the input image (of sensor readings) to the output image (of Gaussian distributions for TX locations). We refer to this as the *image-to-image translation* model. Our approach is inspired by the recent work [9] that frames a different wireless localization problem as an image-to-image translation problem. We incorporate the idea into our multiple transmitter localization problem and utilize recent advances in the computer vision area. Encoder–decoder based CNN models like U-Net [16] with down-sampling and up-sampling convolutional layers have been successful in effectively learning image-to-image translation functions. However, in our setting, we observe that the usage of down-sampling layers (such as max-pooling) degrades the performance of the model, especially in the case when transmitters
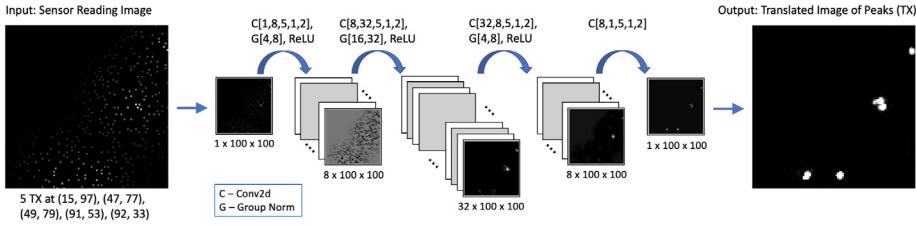
Fig. 4. Architecture of the first step CNN, a four layer image-to-image translation model (`sen2peak`). The figure displays how the data volume flows through the various convolutional layers. C stands for Conv2d, and for each Conv2d layer, the five values shown are [number of input channels, number of output channels, kernel size, stride, padding]. G stands for group normalization, and, for each group normalization, the two values shown are [number of groups, number of channels]. See Section 3 for details.

may be close to each other wherein the model is unable to distinguish the nearby transmitters and generate a single large distribution in the output image. To circumvent this, we avoid using any down-sampling layers in our model and redesign the image-to-image translation model as described below.

`sen2peak` **CNN Model**. We refer to our image-to-image translation CNN model as `sen2peak`, as it translates sensors' readings to "peaks" with Gaussian distributions corresponding to transmitter locations. It has four[3] convolutional layers, as shown in Fig. 2(a). We use an input size of 100×100. The number of convolutional filters are varying for different layers, with up to 32 in one of the layers. We tried doubling the filter numbers at each layer, but it does not lead to significant improvement (it does yield a lower error, but the output image does not improve significantly to impact the second step of our architecture). We use a kernel size of 5×5, a stride of 1, and a padding of 2. This ensures that the dimensions do not decrease and all the pixels are treated uniformly, including the ones at the edge of the image. With the above four convolutional layers, the receptive field [17] of each neuron in the output layer is 17×17. Normalization layers can improve the learning process. We chose group normalization [18] and put it after the first three convolutional layers. We compared group and batch normalization [19] methods in our context, and observed better performance with the group normalization. For the activation layers, we select rectified linear unit (ReLU) and put it after the group normalization layers.

The Loss Function. Our inputs (X) and output (Y) are images. We use L2 loss function which computes the mean squared error aggregated over individual pixels. More formally, our loss function is defined as:

$$\frac{1}{N} \sum_{i}^{N} \|\texttt{sen2peak}(X_i) - Y_i\|^2 \tag{1}$$

where N is the number of samples used in computing the loss, $\|\cdot\|^2$ is L2 loss function, X_i and Y_i are the i_{th} sample's input and output images respectively, and $\texttt{sen2peak}(X_i)$ is the predicted output image corresponding to the input X_i. During training, we use Adam [20] as the optimizer that minimizes the loss function. We set the learning rate to 0.001 and the number of epochs to 20 and the model converges well.

4. `DeepMTL` step 2: TX locations' distributions to precise locations

In this section, we present the second step of our overall localization approach. We refer to this step as the *peak detection* step, as the goal is to detect the peaks within the Gaussian distributions in the input image (which is also the output image of the first step). The first step outputs an image that has multiple distributions (presumably, Gaussian), whose peaks need to be interpreted as precise locations of the transmitters/intruders. As, our end goal is to determine the precise locations of the present transmitters, we develop techniques to detect peaks within the output image of the first step. We propose two different strategies for the peak-detection task. The first strategy is a straightforward peak detection algorithm based on finding local maximal values, while the second strategy is based on framing the problem as an object detection task; for the second strategy, we utilize a widely used state-of-the-art computer vision model called YOLOv3 [14].

Simple Peak Detection Method. The simple and straightforward peak detection method is to designate pixels with locally maximal values as peaks, subject to certain thresholds. More formally, we use a threshold x for a peak value, and also use a parameter r to define a r-radius neighborhood of a pixel. Then, any pixel whose value is more than x and is the maximum among all pixels with a r-radius neighborhood, is designated as a peak (transmitter location). We use $x = 2$ and $r = 3$, in our evaluations. Note that each pixel represents a subarea; thus, a pixel designated as pixel only implies the transmitter

---

[3] We observe that a four-layer lightweight and symmetric `sen2peak` model produces good results and adding more layers gives marginal improvement.
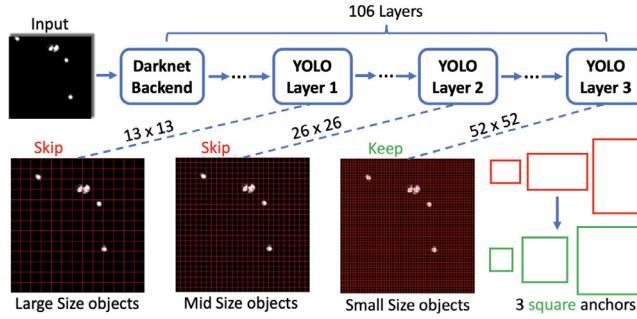
Fig. 5. Our `YOLOv3-cust` in the second step of the `DeepMTL`. The two major customization are: (i) Use only the third YOLO layer that detects small size objects (the output of `YOLOv3-cust` is the bounding box predicted by the third YOLO layer and we use the center of the bounding box as the transmitter location), and (ii) change the rectangle anchors to square anchors.
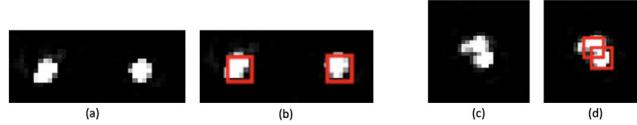

Fig. 6. (a) is the zoom-in of two peaks at the bottom of Fig. 2 example. (c) is the zoom-in of the two close by peaks in the middle right of Fig. 2 example. (b) and (d) shows the bounding boxes that `YOLOv3-cust` outputs for (a) and (c) respectively.

location at the *center* of the corresponding subarea. To localize the transmission more precisely with the pixel's subarea, we use a scheme that localizes the transmitter within the subarea by computing a weighted average of the peak pixel's coordinate and the peak's neighbor pixels' coordinates. The weight of a pixel is the predicted pixel value itself from the first step `sen2peak`. We refer to the above simple approach for the second-step of `DeepMTL` as `simplePeak`.

4.1. Object-detection based precise localization: `YOLOv3-cust`

The simple hand-crafted method described in the previous subsection performs reasonable well in most cases in our simulations. However, its key drawback is that it needs appropriate threshold values that may vary from case to case; such thresholds can be difficult to determine, especially since the input images (with distributions) are not expected to be perfect as they are themselves output of a learning model. Inaccurate threshold values can lead to false alarms and misses. Also, the previous method is not sufficiently accurate at the sub-pixel level, where each pixel may represent a large area such as 10 m $\times$ 10 m or even 100 m $\times$ 100 m. Thus, we propose a CNN-based learning method that overcomes the above shortcomings. CNN has been widely used for object detection in different areas [21,22].

We frame this problem as an object detection task where the objective is to detect and localize known objects in a given image. We observe that our second-step peak detection problem is essentially an object detection problem where the "object" to detect is a "peak". Thus, we turn the `MTL` problem of localizing multiple transmitters into detecting peaks in the images output by `sen2peak` model. For object/peak detection, we design `YOLOv3-cust`, our customized version of YOLOv3 [14]. Fig. 6 is a zoom-in of localizing two close by transmitters (peaks) in Fig. 2(b).
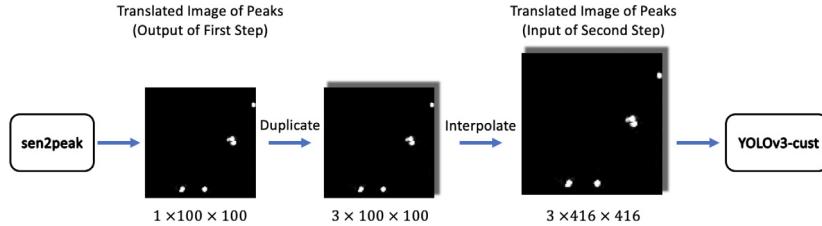
Peak Detection Using `YOLOv3-cust`. Object detectors are usually comprised of two parts: (i) a backbone which is usually pre-trained on ImageNet, and (ii) a front part (head), which is used to predict bounding boxes of objects, probability of an object present, and the object class. For the front part, object detectors are usually classified into two categories, i.e., one-stage detectors such as the YOLO [23] series, and two-stage detectors such as the R-CNN [24] series. We choose the one-stage YOLO series because of its computational efficiency, high popularity and available ways to customize it for our specific context. We refer to the customized version as `YOLOv3-cust`, see Fig. 5. Implementing a 106-layer deep neural network with a complex design from scratch is out of scope of our work. Thus, we use a publicly available source repository [25] and made customization on top of it. We refer to the architecture that uses `sen2peak` and `YOLOv3-cust` in sequence as `DeepMTL`, our key product. In addition, we use `sen2peak` in combination with the uncustomized original YOLOv3, and refer to it as `DeepMTL-yolo` (still change the class number to one).

Customization of YOLOv3. Overall, we incorporated four customization to YOLOv3, of which two are significant and the other two are relatively minor. See Table 1. YOLOv3 is designed to be a general object detector that can detect objects of various sizes, shapes, and classes within input images of various sizes. However, in our context, the input images are of a fixed size, with only a single class of objects which are relatively small and semi-circular. Based on the above observations, we make changes to the original YOLOv3 that both decrease the model complexity and improve its performance.

Table 1
Differences between the original YOLOv3 and our YOLOv3-cust.

YOLOv3	YOLOv3-cust
Has three YOLO layers at 13 × 13, 26 × 26, and 52 × 52 for detection	Only use the last 52 × 52 YOLO layer for detection (skip the first two YOLO layers)
Has 3 different rectangle anchors for each YOLO layer	Has 3 square anchors
Every 10 batches, randomly chooses a new input image dimension size	Do not randomly choose new input dimension size
Has 80 different categories of object class	Only has one category for the peak class

Fig. 7. The data processing of sen2peak's output to get YOLOv3-cust's input of correct size.

Customization Details. The first and second changes presented in Table 1 are major changes and we elaborate them in the following paragraphs. Making prediction at three different scales is one of the highlights of YOLOv3 and an improvement comparing to the previous version YOLOv2 which was prone to missing at detecting small objects. As shown in Fig. 5, the coarse-grain 13 × 13 YOLO layer-1 is designed for detecting large size objects, the 26 × 26 YOLO layer-2 is designed for detecting middle-sized objects, and the fine-grained 52 × 52 YOLO layer-3 is designed for detecting small-sized objects. Since the peaks in our translated images are always small objects, we only use the last 52 × 52 YOLO detection layer (and skip the first two YOLO layers). As shown in Fig. 5, by "skipping" the two YOLO layers means that we do not use them in computing the overall loss function and their outputs are not used in predicting the bounding boxes. In our YOLOv3-cust, the only YOLO layer predicts 8112 bounding boxes, since it has a dimension of 52 × 52 and each cell results in prediction of 3 bounding boxes; this is in contrast to the original YOLOv3, which predicts 10 647 bounding boxes ($3 \times (13 \times 13 + 26 \times 26 + 52 \times 52) = 10647$).

The anchor box is one of the most important hyperparameters of YOLOv3 that can be tuned to improve its performance on a given dataset. The original YOLO's anchor boxes are 10 × 13, 16 × 30, and 33 × 23 (for the input image of size 416 × 416 pixels), which are essentially bounding boxes of a rectangular shape. These original YOLOv3 anchors were designed for the Microsoft COCO [26] dataset, and were chosen since they best describe the dimensions of the real world objects in the MS COCO dataset. In our context, since the peaks are generally squares—we use the anchor boxes to be 15 × 15, 25 × 25, and 35 × 35.

Input Image for YOLOv3-cust. The first step sen2peak's output image is 100 × 100, while the second step YOLOv3-cust's input is required[4] to be a three-channel (RGB) image with each channel being size of 416 × 416. To feed the output of sen2peak to YOLOv3-cust, we do the following: (i) First, we duplicate the sen2peak's output image to create two more copies and thus create a three-channel image of 100 × 100 size channels; (ii) Next, we resize the 100 × 100 channels to 416 × 416 channels using the PyTorch's default "nearest neighbor" interpolation. See Fig. 7.

Output of YOLOv3-cust. YOLO treats objected detection as a regression problem. The regression target (or "label") for an object is a five-value tuple (x, y, *length*, $width$, *class*). In our case, there is only one *class*. x and y are real number location coordinates of the center of the bounding box, which we use as the location of the transmitter. *Width* and *height* determine the size and shape of the object—which we consistently set to be 5 each to signify a 5 × 5 square. Note that the center of the bounding box is in the continuous domain. Thus, we are able to get sub-pixel level location of the transmitters.

5. Localization in the presence of authorized users

Till now, we have assumed that the only transmitters present in the area are the intruders which need to be localized. In this section, we solve the more general MTL problem, where there may be a set of authorized users in the background. This is referred to as the multiple transmitter localization - shared spectrum (MTL-SS) problem [6].

In particular, in a shared spectrum paradigm, there are primary users and an evolving set of active secondary users transmitting in the background. Different than the intruders whose locations are unknown, the authorized users' locations

---

[4] YOLOv3 was developed before our work and the YOLOv3 authors set the input size of the CNN model to 3 × 416 × 416. Although we are customizing their YOLOv3 model, we cannot change the input size because changing it will change the convolutional layer structure, which will preclude us from using the pre-trained weights in the YOLOv3 backbone.
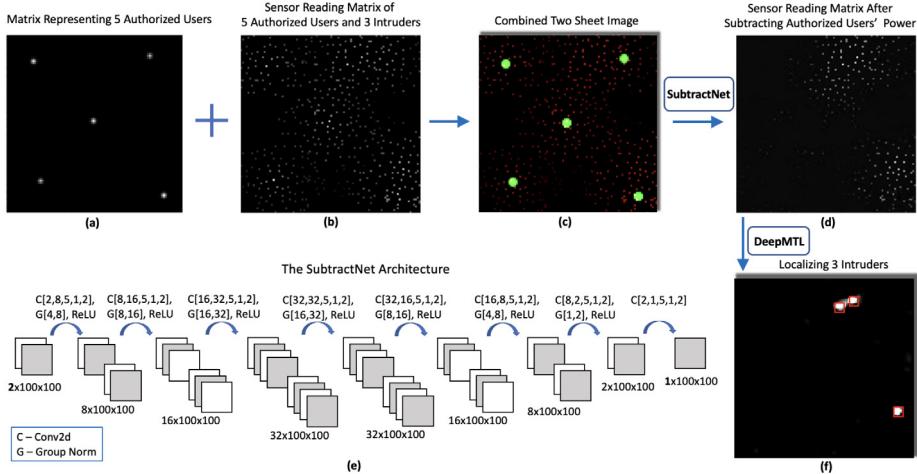
Fig. 8. Overall architecture of second approach to localize 3 intruders in the presence of 5 authorized users. The input of the `SubtractNet` is (c), which is stacking authorized user matrix (a) and the sensor reading matrix (b). (d) is the output of `SubtractNet`, where the transmission power of the authorized users is subtracted from the area. The details of the `SubtractNet` model is in (e). (f) is the localization output after feeding (d) into `DeepMTL`.

are known and we wish to utilize this known information to better localize the unknown intruders. The key challenges come from the fact that the set of authorized users is not static and changes over time as allocation requests are granted and/or active secondary users become inactive over time. A straightforward way to handle background authorized users is to localize every transmitter, and then remove the authorized users. However, any localization approach is susceptible to performance degradation with the increase in the number of transmitters to be localized. Thus, the straightforward approach of localizing every transmitter is likely to be error-prone. Therefore, we attempt to develop a new approach that uses `DeepMTL` as a building block that uses the information of the location of the authorized uses in a way other than removing them after localizing all. The new approach tries to subtract the received signal strength at the sensors by a value received from the authorized users. This subtraction is done by a novel CNN model; we refer to it as `SubtractNet`. Then we feed the image with subtracted powers to the `DeepMTL` and get the locations of the intruders. See Fig. 8(c)–(d)–(f). We describe `SubtractNet` in the following paragraphs.

SubtractNet Input Image. The sensor reading has two sources, one is the intruders and the other is the authorized users. We aim to subtract the power of the authorized users and remain the power from the intruders. So the input of the `SubtractNet` will contain two kinds of information: the authorized users' information (Fig. 8(a)), including both the location and the transmitter power, and the sensor reading matrix (Fig. 8(b)) that encode the power from all transmitters. To incorporate the two kinds of information, we first encode the authorized user information into a matrix that has the same dimension as the sensor reading matrix. Then stack the two matrices together. The combined stacked image is nothing but a two-channel image, which can be interpreted as Red and Green channels. The sensor reading matrix is the Red channel and the authorized user matrix is the Green channel. There is no Blue channel. To represent the authorized transmitter in the Green channel, we use a Gaussian peak similar to what we did in the `sen2peak` for representing transmitters (Section 3). The difference is that in `sen2peak`, all the peaks have a uniform height, whereas in `SubtractNet`, the height of the peak is the power of the authorized transmitter. So the higher the power of the authorized transmitter, the higher the peak in the Green channel. Another difference is that the authorized transmitters are approximated at discrete locations instead of the continuous locations as in `sen2peak`.

SubtractNet Output Image. The `SubtractNet`'s output image is just a one-channel images and represents the sensor readings due to the intruders only.

SubtractNet CNN Architecture. We refer to the model that subtracts the power from the authorized users as the `SubtractNet`. It has a similar design philosophy with `sen2peak`. `SubtractNet` is also an image-to-image translation neural network. Compared to `sen2peak`, it doubled the number of layers, mainly because `SubtractNet` needs a bigger receptive field than `sen2peak`. A bigger receptive field can let the CNN model update sensors that are further away from the authorized user. For the loss function, we use the L2 loss function, similar to the loss function used in Eq. (1), merely replacing the `sen2peak` with `SubtractNet` in Eq. (1). The training details are also the same as in `sen2peak`.

6. Estimating the transmit power of transmitters

In this section, we extend our techniques to estimate the transmit power of the intruders; we refer to the overall problem as Multiple Transmitter Power Estimation (MTPE). Estimation of the transmit power of transmitters can be very

useful in the shared spectrum systems. In particular, estimated transmit powers of the primary users (if unknown, as in the case of military users or legacy systems) can be used to set a "protective" region around them—inside which secondary users can be disallowed [27]. Estimating transmit power of secondary users can also be useful. E.g., if the violation in a shared spectrum system is based on a certain minimum threshold, then it is important to estimate the transmit power to determine a violation. Also, the estimated transmit power of secondary users can also be used to "circumvent" their intrusion—i.e., for the primary users to appropriately increase their transmit power to overcome the harmful interference from the secondary users. In general, estimating the transmission power is beneficial to various operations such as node localization, event classification, jammer detection [28].

There are several works that estimates the transmission power of a single transmitter, often jointly with its location [27–29]. Our previous work [6] can estimate the power of multiple transmitters. The similarity among all four of these methods is that they are estimating the power and location jointly. In this paper, we propose a new method that leverages the capabilities of DeepMTL by using it as a building block. We first localize the transmitters by DeepMTL. Then given the localized locations, estimate the transmitters' transmission power by a newly designed CNN model PredPower. Although PredPower is designed to only estimate the power of a single transmitter, we use it together with a machine learning-based error correction method that can mitigate the errors while applying PredPower to the multiple transmitter power estimation scenario.

In this section, we develop a technique to predict the transmission powers of the intruders. Here, for simplicity, we assume no background authorized users, though, the techniques in this section also work in the presence of authorized users. We leverage our accurate and robust localization solver that tolerates varying transmission power for different transmitters (the varying transmission power needs to be in a range). We propose an efficient approach and its overall methodology at a high-level is as follows. And then in the next subsection we describe our PredPower model.

1. We use DeepMTL to localize the multiple transmitters in a field.
2. We develop a CNN model PredPower to predict power of a single isolated (far away from other intruders) intruder.
3. For other (non-isolated) intruders, we still use PredPower to predict their powers but employ a post-processing "correction" technique to account for nearby intruders.

6.1. PredPower: Predicting power of a single isolated TX

PredPower Input Image. Let us consider an "isolated" transmitter T. To predict T's power, we start with creating a smaller-size image by cropping the original sensor readings image with the area of a certain size around T. In our evaluations in Section 7, the transmitters have a transmit radius[5] of around 20 pixels, which is equivalent to 200 m.[6] For this setting, we used an cropped area of 21×21 around the isolated transmitter T to predict its power, with T is at the center of this area; also, in this setting, we define a transmitter to be *isolated* if there is no other transmitter within a 20-pixel distance.[7] Note that the above cropping process requires the location of the transmitter to be known, and hence, we undertake the above power-estimation process after the localization of the transmitters using the DeepMTL model. We crop images from the same dataset where DeepMTL is trained on.

PredPower Output Power. The output of the PredPower is a single pixel whose value is the predicted power of the transmitter located at the center of the cropped image. Before coming into this single pixel output design, we tried using the height or radius of the peak from the output of sen2peak to indicate the power. But we figure out that the height or radius of the peak is hard to accurately predict and therefore is not an accurate indicator of the power. So we reduced the output complexity and designed the output as a simple single pixel whose value directly represents the power of the transmitter. By simplifying both the input side and output side, we can design and implement a novel CNN model that can accurately predict the power of a single transmitter, as described in the following paragraph.

PredPower CNN Architecture. We refer to our CNN model that estimates the power of a single transmitter as PredPower. See Fig. 9. It has a similar design to sen2peak as well, where it has no max-pooling layers and no fully connected layers. We do not use the fully connected layers and design a fully-convolutional network since the usage of fully connected layers will destroy the spatial relationships. PredPower has five CNN layers and each CNN layer has a kernel size 5×5, striding 1 and padding 0. With this setting, a pixel in the output layer has a receptive field of 21×21, which is exactly the size of the input cropped image. Also note that the pixel is exactly at the location where the transmitter is assumed to be located (recall that the transmitter is at the center of the cropped image). We tried both batch normalization and group normalization and found that batch normalization is better than group normalization, which is the opposite to the sen2peak scenario. ReLU is used as the activation function.

---

[5] I.e., sensors beyond a distance of 20 pixels away from a transmitter x receive only negligible power from x.

[6] Transmission ranges of a standard 2.4 GHz and 5 GHz WiFi at default transmission powers (100 mW) are roughly 45 m and 15 m respectively. In our simulations (Section 7), we use the 600 MHz frequency band. As the lower the signal frequency, the higher the transmission range, a transmission range of around 200 m is reasonable.

[7] Ideally, transmitters with a transmit radius of 20 pixels should entail defining isolated transmitters as ones that have no other transmitters within a 40-pixel distance, and then use a 41×41 area around the isolated transmitter. However, in our evaluations, our chosen values yielded a more efficient technique with sufficient accuracy.
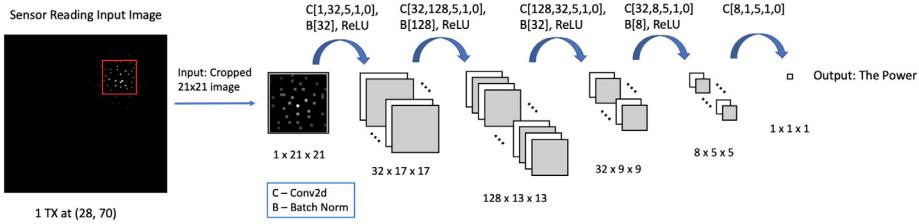
Fig. 9. Architecture of the `PredPower`, a five-layer CNN model that takes in a cropped image from the original input image and outputs the predicted power of one transmitter. The figure displays how the data volume flows through the various convolutional layers. C stands for Conv2d, a 2D convolutional layer, and for each Conv2d layer, the five values shown are [number of input channel, number of output channel, kernel size, stride, padding]. B stands for batch normalization 2d, and for each batch normalization, the value shown is [number-of-features].

Loss Function. The output of the last convolutional layer is technically a 3D cube, although $1 \times 1 \times 1$. So we flatten it in the end to get one scalar value. We use a L2 loss function, which is formally defined as:

$$\frac{1}{N} \sum_{i}^{N} (\texttt{PredPower}(X_i^c) - y_i)^2, \tag{2}$$

where N is the number of training samples, X_i^c is the cropped input image for the ith sample and y_i is the ground truth power for the ith sample. $\texttt{PredPower}(X_i^c)$ is the predicted power. We use Adam as the optimizer, and set the learning rate to 0.001 and the number of epochs to 20, which is sufficient for the model convergence.

6.2. Estimating powers of multiple transmitters

Our end goal is to estimate the power of multiple transmitters at the same time. When the multiple transmitters are far away and isolated from each other, the problem reduces to single transmitter power estimation, which `PredPower` handles well. The hard part is to estimate transmit power of multiple transmitters that are close by. In this case, a sensor will receive an aggregated power from multiple transmitters. We assume that blind source power separation is not viable.

Overall High-Level Approach. For each localized intruder by using `DeepMTL` (whether isolated or not), we crop the 21×21 size area around it and feed it to `PredPower`, and estimate its power. If it is actually isolated, then the predicted power is final. If it is not isolated, then we apply a post-processing correction phase to account for the overestimation of the powers, as described below.

Correction Method for Close by Transmitters. Let us first consider the case where there are two close by transmitters T_0 and T_1. We use `PredPower` to estimate the power of two transmitters and get p_0' and p_1' respectively. Let us say the ground truth are p_0 and p_1 respectively. The estimated power will most likely be higher than the ground true power, i.e., $p_0' > p_0$ and $p_1' > p_1$. Because `PredPower` can only "see" one transmitter, and it will view two transmitters in the areas as a combined single one. Let us focus on T_0 and assume $\delta_0 = p_0' - p_0$. The intuition is that δ_0 has some underlying patterns that we are able to recognize. We model δ_0 as a function of some features related to T_0 and T_1. We model δ_0 as follows,

$$\delta_0 = \theta_0 \cdot p_0' + \theta_{(1,1)} \cdot d_{01} + \theta_{(1,2)} \cdot p_1' + \theta_{(1,3)} \cdot \frac{p_1'}{d_{01}} \tag{3}$$

where d_{01} is the distance between T_0 and T_1, and the four θs are the coefficients for the four terms respectively. The first term is related to T_0 itself, and the other three terms are related to T_1. We observe that the smaller the d_{01}, the larger the value of δ_0. And the bigger the p_1', the larger the value of δ_0. So d_{01} has a negative correlation with δ_0 while p_1' has a positive correlation. $\frac{p_1'}{d_{01}}$ is a combination of two terms to increase the number of features. We also tried a few other features, but we decided to use only these three features for a close by transmitter as a balance of model accuracy and model complexity.

Eq. (3) is for the case of one close by transmitter, we then extend the equation to handle multiple close by transmitters in the following Eq. (4),

$$\delta_0 = \theta_0 \cdot p_0' + \sum_{i=1}^{m} (\theta_{(i,1)} \cdot d_{0i} + \theta_{(i,2)} \cdot p_i' + \theta_{(i,3)} \cdot \frac{p_i'}{d_{0i}}) \tag{4}$$

where m is the number of close by transmitters for T_0, the transmitter of interest, d_{0i} is the distance between T_0 and close by T_i, and p_i' is the uncorrected power predicted by `PredPower`. For the ith close by transmitter, we introduce three terms $d_{0i}, p_i', \frac{p_i'}{d_{0i}}$, and assign three coefficients $\theta_{(i,1)}, \theta_{(i,2)}, \theta_{(i,3)}$ to the three terms respectively. So for m close by transmitters, there are $1 + 3m$ number of terms in the equation.

After modeling δ_0, in Eq. (5), we "correct" p'_0 by subtracting δ_0 from p'_0 to get an more accurate estimation of the power of transmitter T_0.

$$p_0^{correct} = p'_0 - \delta_0 \tag{5}$$

Estimating the parameter θ. Eq. (4) is essentially a linear model and we can train it by using either linear, ridge, or LASSO regression models [30]. We perform experiments using ridge regression (alpha=0.01). We set a distance threshold for a neighbor transmitter to be classified as a close by transmitter. Note that the transmitters will have a different number of close by transmitters. So, let us denote M as the maximum number of close by transmitters we see in the dataset. When training the linear model in Eq. (4), we train a model that assumes a maximum M number of close by transmitters, i.e., the linear model has $1 + 3M$ terms. The $3M$ terms are organized in a group of three (i.e., three features) and the groups are sorted by distance in an ascending order. Then, for a transmitter with a smaller than M number of close by transmitters, let us say m, only the first $1 + 3m$ terms will have a meaningful value. And for the rest $3(M - m)$ terms, we set the value to zero, i.e., impute missing value with zero.

7. Evaluation

To evaluate the performance of our proposed techniques, we conduct large-scale simulations over two settings based on two different propagation models. In particular, we consider the log-distance-based propagation model and the Longley–Rice model obtained from SPLAT! [31]. We evaluate various algorithms, using multiple performance metrics as described below.

Performance Metrics. We use the following metrics 1, 2, and 3 to evaluate the localization methods and use the 4th metric to evaluate the power estimation methods.

1. Localization Error (L_{err})
2. Miss rate (M_r)
3. False Alarm rate (F_r)
4. Power Error (P_{err})

Given a multi-transmitter localization solution, we first compute the L_{err} as the minimum-cost matching in the bi-partite graph over the ground truth and the solution's locations, where the cost of each edge in the graph is the Euclidean distance between the matched ground truth node location and the solution's node location. We use a simple greedy algorithm to compute the min-cost matching. The unmatched nodes are regarded as false alarms or misses. We also put an upper threshold on the cost (L_{err}) of an eligible match. E.g., if there are four intruders in reality, but the algorithm predicts six intruders then it is said to incur zero misses and two false alarms, so the M_r is zero and the F_r is one-third. If the algorithm predicts three intruders then it incurs one miss and zero false alarms, so the M_r is one-fourth and the F_r is zero. In the plots, we stack the miss rate and false alarm rate to reflect the overall performance.

Algorithms Compared. We implement[8] and compare six algorithms in two stages. In stage one, we compare three versions of our techniques, viz., `DeepMTL`, `DeepMTL-yolo`, and `DeepMTL-peak`. Recall that `DeepMTL`, `DeepMTL-yolo`, and `DeepMTL-peak` use `sen2peak` in the first step, and `YOLOv3-cust`, original `YOLOv3`, and `simplePeak` respectively in the second step. In the first stage of our evaluations, we will show that `DeepMTL` outperforms `DeepMTL-yolo` and `DeepMTL-peak` in almost all performance metrics. Thus, in the second stage, we only compare `DeepMTL` with schemes from three prior works, viz., SPLOT [5], `DeepTxFinder` [7], and MAP* [6] and show that `DeepMTL` outperforms the prior works.

Training and Testing Dataset. We consider an area of 1 km × 1 km, and use grid cells (pixels) of 10 m × 10 m, so the grid is 100 × 100. The transmitters may be deployed anywhere within a cell (i.e., their location is in the continuous domain), while the sensors are deployed at the centers of the grid cells (i.e. their location is in the discrete domain). For each instance (training or test sample), the said number of sensors and transmitters are deployed in the field randomly. For each of the two settings (propagation models described below), we create a 100,000 sample training dataset to train our models and create another 20,000 sample testing dataset to evaluate the trained model.

We will evaluate the performance of various techniques for varying number of transmitters/intruders and sensor density. When we vary a specific parameter, the other parameter is set to its *default* value; the number of transmitters varies from 1 to 10 and the default value is 5; the sensor density varies from 1% to 10% and the default value is 6% (600 sensors in a 100 × 100 grid). The two default numbers 5 and 6% are chosen because they are in the middle of their ranges. When not mentioned, the default values are used. The transmitter power varies from 0 to 5 dBm and is randomly picked. To minimize overfitting, the training dataset and testing dataset have sensors placed at completely different locations.

We train the `DeepMTL` model using the 100,000 sample dataset. To train `DeepTxFinder` [7], we partition the 100,000 sample training dataset into ten datasets based on the number of transmitters in the samples which varies from 1 to 10.
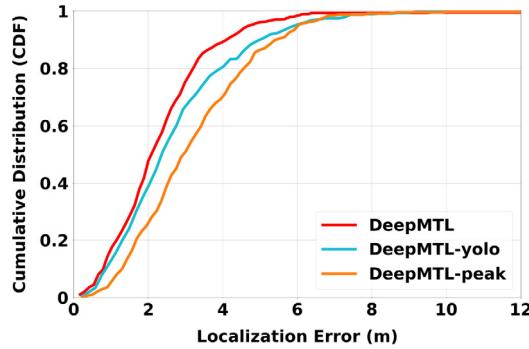
---

[8] Source code at: https://github.com/caitaozhan/deeplearning-localization.

Fig. 10. Cumulative probability of localization error of `DeepMTL`, `DeepMTL-yolo` and `DeepMTL-peak`, for the special case of single transmitter localization with 6% sensor density.
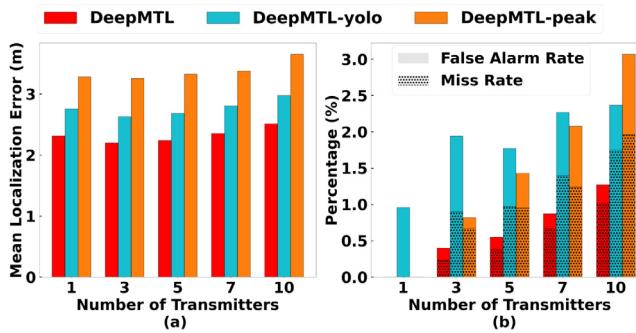

Fig. 11. (a) Localization error and (b) miss and false alarm rates, of `DeepMTL`, `DeepMTL-yolo` and `DeepMTL-peak` variants for varying number of transmitters in log-distance dataset/propagation model.

These ten datasets are used to train the ten "localization" CNN models in `DeepTxFinder`, and the full dataset of 100,000 samples is used to train the `DeepTxFinder` model that determines the number of transmitters. For the `MAP*` scheme [6], we assume the availability of all required probability distributions. We note that using a simple cost model (number of samples need to be gathered), the overall training cost for `MAP*` is an order of magnitude higher than `DeepMTL` and `DeepTxFinder`. Lastly, SPLOT [5] does not require any training.

Two Propagation Models and Settings. The sensor readings (i.e. the dataset) are simulated based on a propagation model. To demonstrate the generality of our techniques, we consider two propagation models as described below.

Log-Distance Propagation Model and Setting. Log-Distance propagation model is a generic model that extends Friis Free space model which is used to predict the path loss for a wide range of environments. As per this model, the path loss (in dB) between two points x and y at a distance d is given by: $PL_d = 10\alpha \log d + \mathcal{X}$, where α (we use 3.5) is the path-loss exponent and $\mathcal{X}$ represents the shadowing effect that can be represented by a zero-mean Gaussian distribution with a certain (we use 1) standard deviation. Power received (in dBm) at point y due to a transmitter at point x with a transmit power of P_x is thus: $P_x - PL_d$. Power received at point y due to multiple sources is assumed to be just an aggregate of the powers (in linear) received from each of the sources.

SPLAT! Model and Setting. This is a complex model of wireless propagation based on many parameters including locations, terrain data, obstructions, soil conditions, etc. We use SPLAT! [31] to generate path-loss values. SPLAT! is an open-source software implementing the Longley–Rice [32] Irregular Terrain With Obstruction Model (ITWOM) model. We consider a random area in Long Island, New York of 1 km × 1 km large and use the 600 MHz band to generate path losses.

7.1. `DeepMTL` vs. `DeepMTL-yolo` vs. `DeepMTL-peak`

In this subsection, we compare the three variants of our technique, viz., `DeepMTL`, `DeepMTL-yolo`, and `DeepMTL-peak`. For simplicity, we only show plots for the log-distance propagation model setting in this subsection (we observed similar performance trends for the Longley–Rice propagation model too).

Performance Results. In Fig. 10, we plot the cumulative density function (CDF) of the localization error, for the simple case of a single transmitter. We observe that `DeepMTL` outperforms the other variants, as it yields a higher cumulative probability
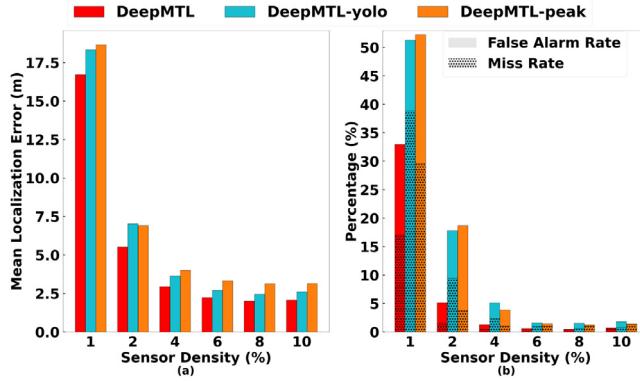
Fig. 12. (a) Localization error and (b) miss and false alarm rates, of DeepMTL, DeepMTL-yolo and DeepMTL-peak variants for varying sensor density in log-distance dataset/propagation model.

Table 2
Compare localization running time (s) for 1 to 10 number of intruders.

Intru.	DeepMTL-peak	DeepMTL-yolo	DeepMTL	MAP*	SPLOT	DeepTxFinder
1	0.0013	0.0180	0.0180	8.78	1.53	0.0015
3	0.0014	0.0183	0.0186	15.1	1.79	0.0016
5	0.0016	0.0192	0.0189	19.3	2.06	0.0017
7	0.0018	0.0196	0.0194	24.1	2.32	0.0019
10	0.0023	0.0205	0.0206	28.5	2.72	0.0022

for a lower range of errors. In addition, we evaluate the three variants for varying number of transmitters (Fig. 11) and sensor density (Fig. 12), and evaluate the localization error as well as the false alarm and miss rates. We observe that DeepMTL consistently outperforms the other two variants across all plots and performance metrics. As expected, the performance of all algorithms degrades with an increase in the number of transmitters (in terms of false alarms and miss rates) or with a decrease in sensor density. In general, the localization error of DeepMTL is around 15%–30% lower than the other variants. Impressively, the total cardinality error (i.e., false alarms plus miss rates) is fewer than 1% for the DeepMTL technique, when the sensor density is 6% or above.

When the sensor density is as low as 1%, the performance of all methods significantly decreases. Because when the sensor density is 1% or lower, the input image will be very sparse and contain only a few pixels. DeepMTL's first part sen2peak has a receptive field of 17×17. This area will contain an average of less than three sensors when the sensor density is 1% ($17 \times 17 \times 0.01 = 2.89$). This number is considered too low and note that 2.89 sensors are not enough for the trilateration localization method, which needs three sensors. Our CNN models need to function well with enough pixels that contain useful information. So we suggest the sensor density to be at least 2% to achieve reasonable results.

Running Time Comparison. For the running time comparison of the variants, see Table 2. Our hardware is an Intel i7-8700 CPU and an Nvidia RTX 2070 GPU. We observe that, as expected, DeepMTL and DeepMTL-yolo which use a sophisticated object-detection method do incur higher latency (around 20 ms) than DeepMTL-peak (around two milliseconds). As our key performance criteria is accuracy and the run time of DeepMTL is still quite low, we choose DeepMTL for comparison with the prior works in Section 7.2.

Localizing Transmitters Close By. Localizing two or more transmitters close by is a hard part of the MTL problem. Fig. 6(c) and (d) gives an example of when an advanced object detection algorithm will work while a simple local maximal peak detection might not. Fig. 6(c) and (d) shows DeepMTL can successfully localize two transmitters as close as three pixels apart. When a pixel represents a 10 m × 10 m area, then it is 30 meters apart. If a pixel represents a smaller area, such as 1 m × 1 m, it has the potential to localize two transmitters as close as three meters apart.

Two YOLO Thresholds. YOLO has two important thresholds to tune that can affect the miss rate and false alarm rate. One is the confidence threshold (conf) and the other is the non-maximum suppression threshold (nms). An object will be recognized as a peak only if its confidence level is larger than conf. If two recognized peaks' bounding boxes have a large overlap, and their intersection of union is higher than nms, then the two peaks will be considered as one peak. The peak with a higher confidence level keeps while the other peak with a lower confidence level discards. A higher conf will bring a lower false alarm rate but a higher miss rate, and a higher nms will bring a lower miss rate but a higher false alarm rate. We pick conf = 0.8 and nms = 0.5 for DeepMTL as we observe these values bring a good balance between false
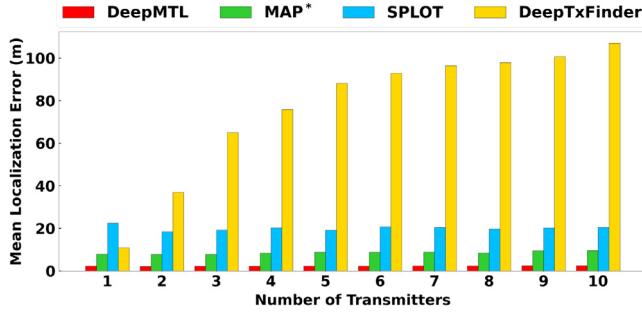
Fig. 13. Localization error of `DeepMTL`, `MAP*`, `SPLOT`, and `DeepTxFinder` for varying number of transmitters in the log-distance dataset.
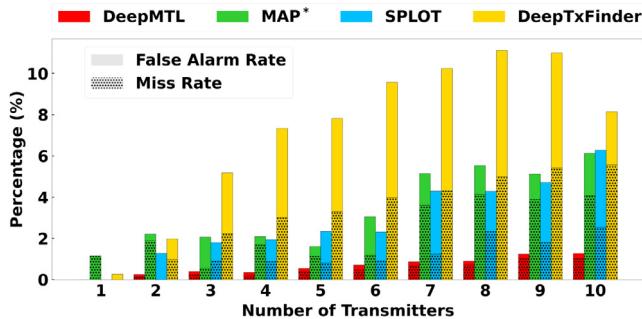

Fig. 14. Miss and false alarm rates of `DeepMTL`, `MAP*`, `SPLOT`, and `DeepTxFinder` for varying number of transmitters in the log-distance dataset.
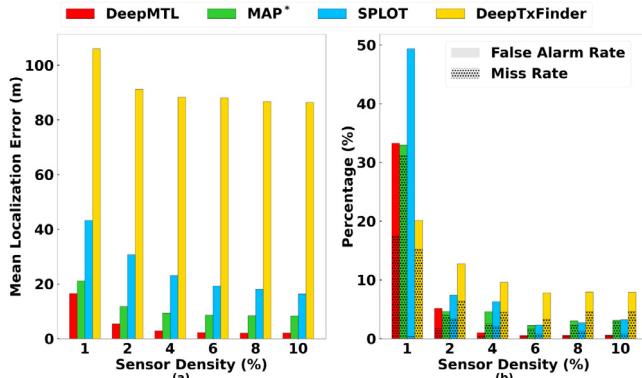

Fig. 15. (a) Localization error, and (b) miss and false alarm rates, of `DeepMTL`, `MAP*`, `SPLOT`, and `DeepTxFinder` for varying sensor densities in the log-distance dataset.

alarm rate and miss rate. In particular, a high `conf` of 0.8 precludes "fake peaks" at locations with no transmitters. Also, a low `nms` weakens `DeepMTL`'s ability to localize two close by transmitters, while a high *nms* yields a high false alarm rate (by incorrectly interpreting a single transmitter as multiple close by transmitters); thus, we chose `nms` of 0.5.

7.2. `DeepMTL` vs. prior works

In this subsection, we compare `DeepMTL` with `SPLOT`, `MAP*`, `DeepTxFinder` in both log-distance (Figs. 13, 14, 15) and SPLAT (Figs. 16, 17, 18) propagation models and thus, datasets. We observe similar performance trends for both datasets, i.e., `DeepMTL` significantly outperforms the other approaches by a large margin (in many cases, by more than 50% in localization errors, false alarms, and miss rates). For all techniques, as expected, the performance is generally worse in the SPLAT dataset compared to the log-distance dataset.
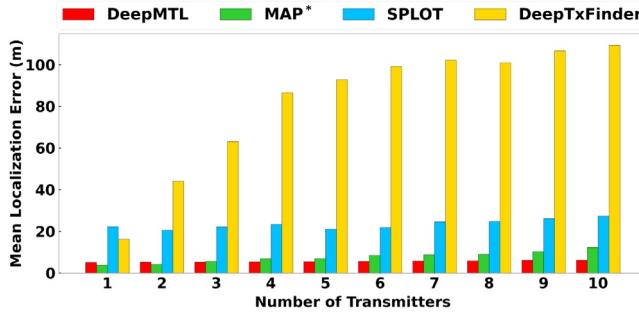
Fig. 16. Localization error of DeepMTL, MAP*, DeepTxFinder and SPLOT for varying number of transmitters in the SPLAT! Dataset.
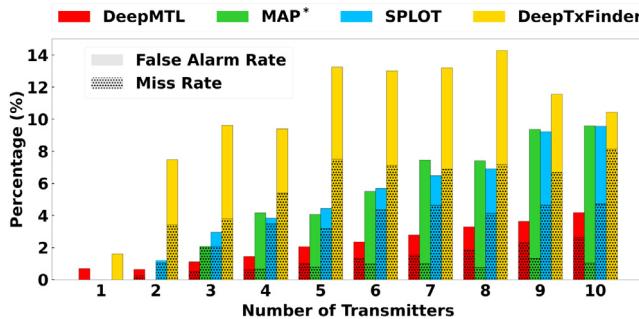

Fig. 17. Miss and false alarm rates of DeepMTL, MAP*, SPLOT, and DeepTxFinder for varying number of transmitters in the SPLAT! Dataset.
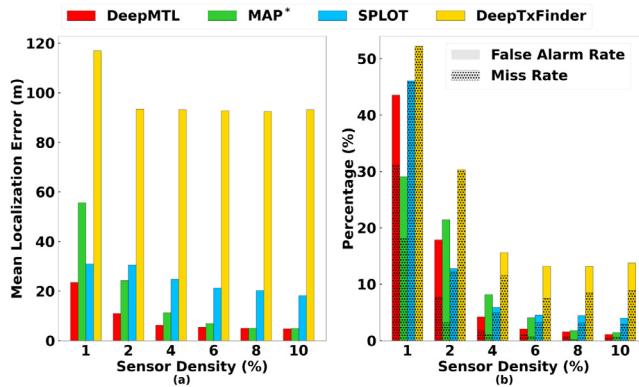

Fig. 18. (a) Localization error, and (b) miss and false alarm rates, of DeepMTL, MAP*, SPLOT, and DeepTxFinder for varying sensor densities in the SPLAT! Dataset.

Varying Number of Transmitters. Figs. 13 and 16 show the localization error with varying number of transmitters, in the two datasets. We see that DeepMTL has a mean localization error of only 2 to 2.5 m (roughly, one-fourth of the side length of a pixel/grid cell) in the log-distance dataset and about 5 to 6 meters in the SPLAT dataset. In comparison, the localization errors of MAP*, SPLOT, DeepTxFinder are two to three times, eight to nine times, and few tens of times respectively more than that of DeepMTL. Figs. 14 and 17 show the miss and false alarm rates with varying number of transmitters in the two datasets. We observe that DeepMTL's summation of miss and false alarm rate is only 1% even at ten transmitters in the log-distance dataset, and about 4% for the case of SPLAT! dataset. In comparison, the summation of miss and false alarm rates for other schemes is at least 6% and 10% respectively for the two datasets, when there are ten transmitters.

Varying Sensor Density. Figs. 15 and 18 plot the performance of various algorithms for varying sensor density in the two datasets. For very low sensor density of 1%, all algorithms perform badly (in comparison with higher sensor densities), but DeepMTL still performs the best except that MAP* performs best at 1% in terms of false alarm rate and miss rate. For
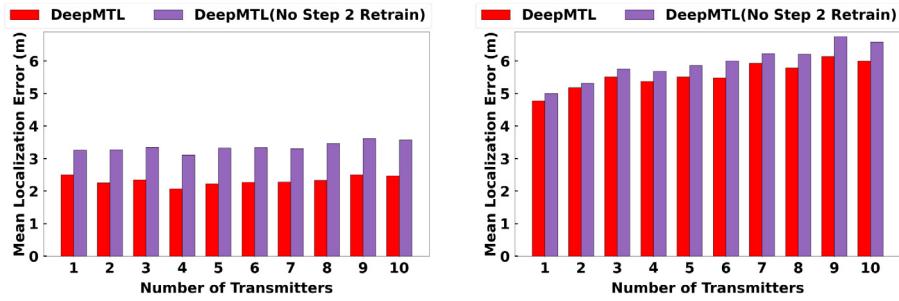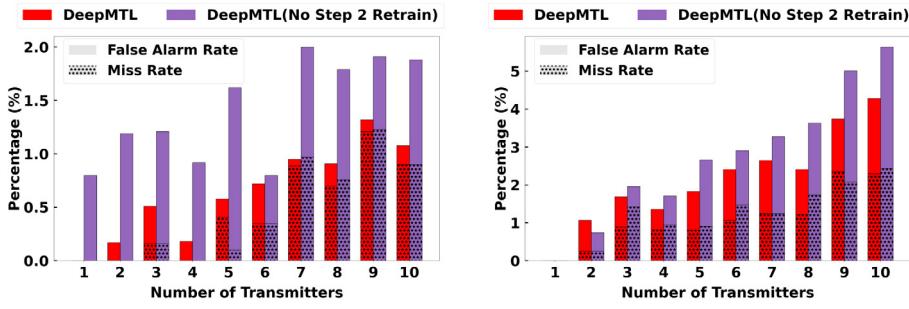
Fig. 19. Localization error for varying number of transmitters when the first and second step of `DeepMTL` are trained on different training dataset.

(a) First step trained in log-distance data, while second step trained in SPLAT! data. Tested on the log-distance data.

(b) First step trained in SPLAT! data, while second step trained in log-distance! data. Tested on the SPLAT! data.

Fig. 20. The miss rate and false alarm rate for varying number of transmitters when the first and second step of `DeepMTL` are trained on different training dataset.

higher sensor densities, we observe a similar performance trend as above—i.e., `DeepMTL` easily outperforms the other schemes by a large margin. For the SPLAT! dataset at the 6% sensor density, the summation of false alarm rate and miss rate is 2%, which is higher than the 1% summation for the log-distance dataset.

Running Times. The run time of `DeepMTL` (in tens of milliseconds) is orders of magnitude faster than `MAP*` and `SPLOT` (both in seconds). See Table 2. The `DeepMTL` run time is an order of magnitude slower than `DeepTxFinder` (in a few milliseconds), due to the deep `YOLOv3-cust` taking up over 90% of the run time.

Summary and Analysis. In summary, our approach significantly outperforms the other approaches in all the accuracy performance metrics, as well as in terms of latency. In particular, our approach also significantly outperforms the other CNN-based approach `DeepTxFinder`. The main reason for `DeepTxFinder`'s inferior performance is its inability to accurately predict the number of TXs—which forms a fundamental component of their technique. In contrast, `DeepMTL` can circumvent explicit pre-prediction of number of transmitters by using a well-developed object-detection technique which works well for multiple objects especially in our context of simple objects.

7.3. Transfer learning

We demonstrate transfer learning (generalizability) by showing that the second step in `DeepMTL` does not need to be retrained for different radio frequency propagation models and terrains. In the previous experiments, the two steps of `DeepMTL` are both trained in the same setting, either log-distance or SPLAT!. We do the following two combinations to show that the second step does not need to retrain:

1. The first step is trained in the log-distance setting and the second step is trained in the SPLAT! setting. Tested on the log-distance data.
2. The first step is trained in the SPLAT! setting and the second step is trained in the log-distance setting. Tested on the SPLAT! data.

In both combinations, the second step `YOLOv3-cust` is trained on a different dataset compared to the first step `sen2peak`. Fig. 19(a) shows that the localization error increases one-third in the first combination compared to the case where both the first and second steps are trained on log-distance dataset. Fig. 19(b) shows that the localization error increases only five percent in the second combination compared to the case where both the first and second steps are trained on SPLAT!
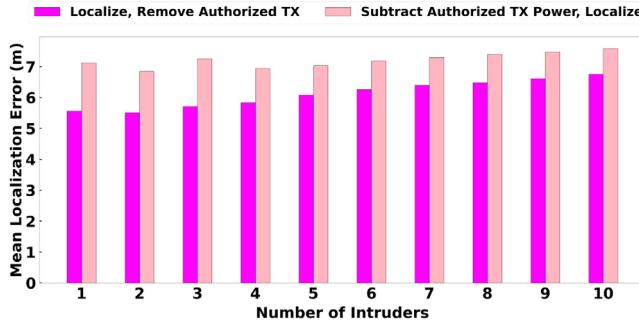
Fig. 21. The localization error of two approaches in the presence of five authorized users with varying number of intruders.
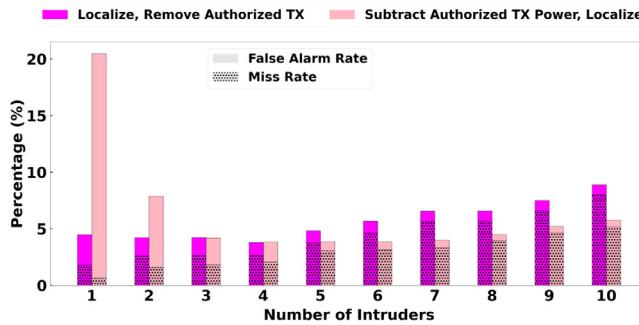

Fig. 22. The miss and false alarm of two localization approaches in the presence of 5 authorized users with varying number of intruders.

dataset. The miss rate and false alarm rate for both combinations also increase minimally, i.e. the summation of miss rate and false alarm rate only increases around 1% in absolute value. See Fig. 20. This implies that the second step of DeepMTL, YOLOv3-cust, is general and does not need to retrain for different radio frequency propagation models and terrains. This is because the first step sen2peak is translating sensor readings images from different geographical areas to the same Gaussian peaks. The first step sen2peak still needs to be retrained for different situations to translate the sensor readings to the peaks.

7.4. Localize intruders in the presence of authorized users

The previous experiment setting is based on the assumption that all transmitters we are localizing are intruders. Different than the previous setting, here, we put five authorized users and they are spread out in the field, so those five will not interfere with each other. This is the more general version of the MTL problem, where there are some authorized users in the background. Fig. 21 shows the localization error of two approaches localizing intruders in the presence of five authorized users with a varying number of intruders. It is observed that the first approach, localize then remove authorized users, has a ten to twenty percent smaller localization error compared to the second approach, subtract authorized user power then localize. This is due to the inaccuracy of power subtraction from the SubtractNet. Fig. 22 shows the miss and false alarm of two approaches localizing intruders in the presence of five authorized users with a varying number of intruders. It is observed that the second approach, subtract authorized TX power then localize, is having a high false alarm when the number of intruders is three or less. So for SubtractNet, subtracting the power of five background authorized users from six transmitters (five out of six transmitters are authorized users, one intruder) is relatively more difficult than subtracting the power of five authorized users from nine users (five out of nine transmitters are authorized users, four intruders). Also statistically, getting one false alarm when there are one intruder and five authorized users is 100% false alarm rate, while getting one false alarm when there are two intruders and five authorized users is only 50% false alarm rate (the denominator is the number of intruders). Thus, the false alarm rate for one and two number of intruders looks to differ a lot, but in reality, the false alarm cases do not differ a lot). When the number of intruders is three or four, the two approaches are comparable. But when the number of intruders is larger than four, the second approach is having a lower miss and false alarm rate. In summary, the two approaches both have their strengths. The main advantage for the second approach is that the sum of miss rate and false alarm rate is lower when the number of intruders is large.
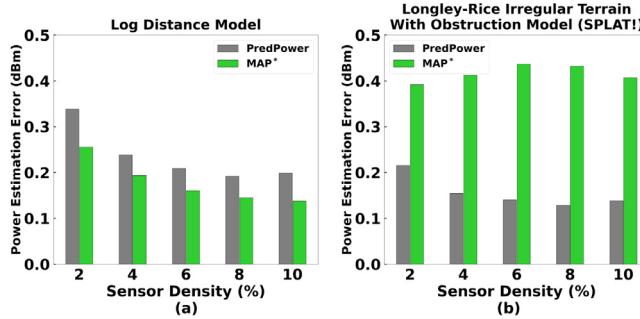
Fig. 23. The single transmitter power estimation error of `PredPower` and `MAP*` in two propagation models, (a) Log-distance model and (b) Longley–Rice Irregular Terrain with Obstruction Model (SPLAT!), for varying sensor densities.
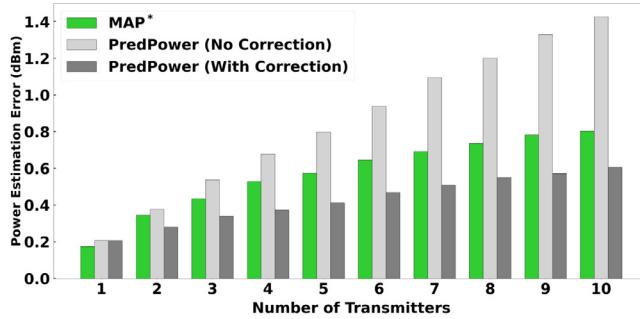

Fig. 24. The transmitter power estimation error of `MAP*`, `PredPower` with and without correction in Log-distance model for varying number of intruders.

7.5. Power estimation evaluation

In this subsection, we evaluate the transmitter power estimation performance. In all experiments, the power range is 5 dB. The power error is presented in absolute value. A power error of 0.5 dB implies a relative power error of 10%. First, we compare the single transmitter power estimation between `MAP*` and `PredPower`, and then compare the multiple transmitter power estimation between `MAP*`, `PredPower` with error correction, and `PredPower` with error correction.

Fig. 23(a) shows the performance of single transmitter power estimation in the log-distance propagation model scenario with varying sensor density. In this case, `MAP*` has a 10 to 20 percent smaller power estimation error. Fig. 23(b) shows the performance of single transmitter power estimation in the SPLAT! model with varying sensor density. In this case, `PredPower` is significantly lower in power error. So in average, `PredPower` outperforms `MAP*` in single transmitter power estimation. We can also conclude that for `PredPower`, a higher sensor density will decrease the power estimation error. While a 2% of sensor density will lead to a higher error, a sensor density of 6% is enough to give relatively good results.

For multiple transmitter power estimation, we compare three methods in two propagation models and show that `PredPower` with error correction has the best performance among the three methods. `PredPower` without error correction is expected to perform the worst and it suggests that the post-processing error correction stage for `PredPower` is important and works well. Fig. 24 shows the power estimation error of three methods with a varying number of transmitters while the sensor density is 6%. In this figure, `MAP*` is the best only when the number of transmitters is one (which is consistent with Fig. 23(a)). Also the number of transmitters is one is the only case when `PredPower` with correction and without correction has the same performance. This is also expected because there is no need to error correction when there is only one transmitter in the area. In all other cases, we see that `PredPower` with error correction is the best, `PredPower` without error correction is the worst, and `MAP*` is in the middle. In Fig. 25, which shows experiment results running in the SPLAT! propagation model, we see a similar pattern compared to Fig. 24. The difference is that `PredPower` with error correction is always the best and the power error is larger than the log-distance model scenario. For example in Fig. 24, the power estimation error for `PredPower` with error correction goes up to 0.6 dB, where as in Fig. 25, the error goes up to 1 dB.
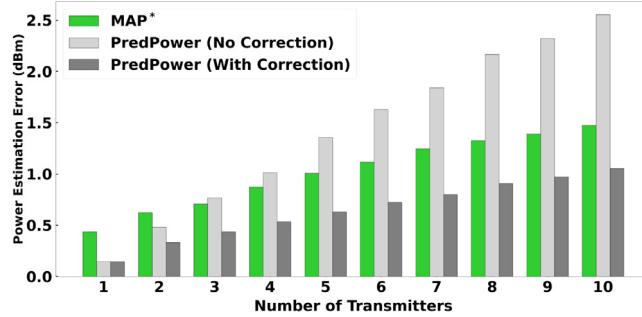
Fig. 25. The transmitter power estimation error of MAP*, PredPower with and without correction in Longley–Rice Irregular Terrain with Obstruction Model (SPLAT!) for varying number of intruders.

7.6. Evaluation over testbed data

In this subsection, we show that our DeepMTL performs well in real-world collected data. For this, we repurpose our testbed data from [6] as described below. We start with describing our testbed data from [6].

Testbed Data. In [6], we conducted a testbed in an outdoor parking area of 32 m × 32 m large.[9] Each grid cell has a size of 3.2 m × 3.2 m, with the grid size being 10 × 10. We place a total of 18 sensors on the ground. The sensors consist of Odroid-C2 (a single-board computer) connected to an RTL-SDR dongle and the RTL-SDR connects to dipole antennas. The transmitters are USRP or HackRF connecting to a laptop. We collect raw Inphase-Quadrature (I/Q) samples from the RTL-SDR at the 915 MHz ISM band. We perform FFT on the I/Q samples with a bin size of 256 samples to get the signal power values, and then utilize the mean and standard deviation of the power at frequency 915 MHz reported from each of the sensors.

Transforming the Data from 10 × 10 to 100 × 100 Grid. Note that DeepMTL's input requires a 100 × 100 input, while the above data is over a 10 × 10 grid. Also, the sensor density in the above data is 18%, while we desire a sensor density of around 4%–6% to have a fair comparison with our simulation based evaluations in previous subsections. To achieve these objectives, we transform the above 10 × 10 data to a 100 × 100 grid data in two steps as follows.

1. Increase the data granularity from 10 × 10 to 20 × 20, by dividing each cell into 2 × 2 cells; we randomly pick one of these four smaller cells to represent the original cell (i.e., to place the sensor if it existed in the original cell). See the red-bordered boxes in Fig. 26(a)–(b). We refer to the full 20 × 20 grid as a *tile*.
2. Now, we duplicate the 20 × 20 tile 25 times using a 5 × 5 pattern to generate a 100 × 100 grid. See Fig. 26(b)–(c).

The above steps effectively increase the area from the original 32 m × 32 m to 160 m × 160 m. Note that the first step above only splits each original cell into four smaller cells without increasing the whole area size. The 100 × 100 grid will have a sensor density of 4.5% and each grid cell represents an area of 1.6 m × 1.6 m.

We note that the second duplication step can introduce inaccurate sensor readings at the tile's "edges", due to any transmitters from adjoining tiles. To circumvent this issue, we place *transmitters* only within the internal 10 × 10 cells of each 20 × 20 tile (i.e., avoid placing a transmitter on the five-cell edge of each tile). This yields a total of 2500 potential positions to place a transmitter in the final 100 × 100 grid. With the above setting, we generate training and testing datasets consisting of 25,000 and 12,500 samples respectively.

Testbed Results. The performance of DeepMTL on this real world based data is shown in Fig. 27. Compared to DeepTxFinder, DeepMTL is significantly better in localization error and false alarm rate and miss rate in almost all cases, which aligns to the results in the previous subsections based on data generated from either log-distance model or SPLAT!. The localization error of DeepMTL in Fig. 27(a) is around 1.3 m. The error increases mildly with the increase in the number of transmitters. The localization error in the testbed data is smaller compared to both log-distance data results (Fig. 13) and SPLAT! data results (Fig. 16). This is because a grid cell here is representing a smaller area. In the log-distance data, the localization error is roughly one-fourth the side length of the grid cell. In the SPLAT! data result, the localization error is roughly half the side length of its grid length. In the testbed data, the localization is roughly eighty percent the side length of a grid cell. So the localization error in the testbed data is the highest relative to the length of a grid cell it represents. The sum of false alarm rate and miss rate is 3% when the number of transmitters is five and is 5% when the number of transmitters is ten. The results are a little bit worse than the results in the SPLAT! data (Fig. 17), where the sum is 2% for five transmitters and 4% for ten transmitters.
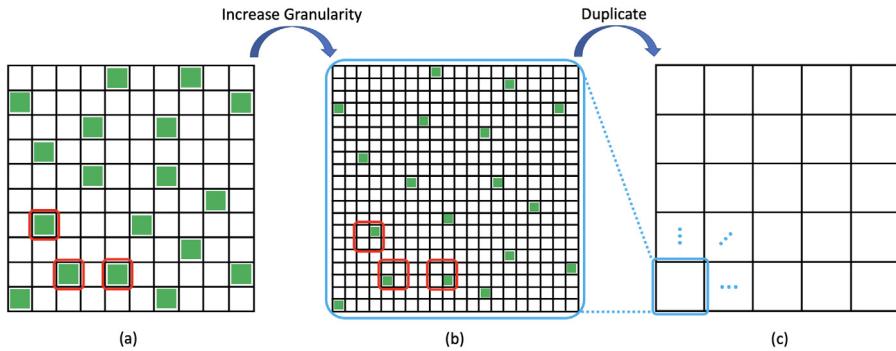
---

[9] Dataset publicly available at: https://github.com/Wings-Lab/IPSN-2020-data.

Fig. 26. (a). The original 10 × 10 testbed grid with 18 sensors (green cells) representing a 32 m × 32 m area. (b). The 20 × 20 grid (a tile) obtained by replacing each original cell by 2 × 2 smaller cells; a sensor, if present in the original cell, is placed in a random cell within the 2 × 2 grid (see the green cells). (c). The final 100 × 100 grid obtained by duplicating the 20 × 20 tile 25 times using a 5 × 5 pattern. The final geographic area is 160 m × 160 m.
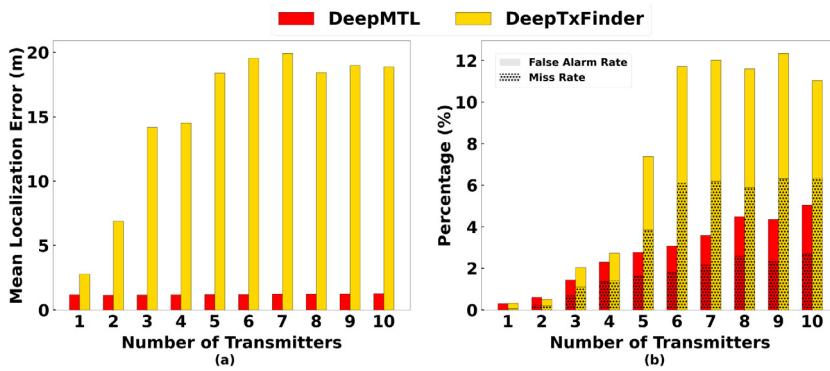

Fig. 27. The localization error (a), false alarm rate and miss rate (b) of DeepMTL and DeepTxFinder in a real world collected data for varying number of intruders.

8. Related work

Spectrum sensing is usually being realized by some distributed crowdsourced low-cost sensors. Electrosense [33] and its follow up work Skysense [34] are typical work of spectrum sensing. In this crowdsourced sensing paradigm [8], sensors collect I/Q samples (in-phase and quadrature components of raw signals) and compute PSD (power spectral density), which is RSS. Crowdsourced low-cost sensors do not have the capability to collect AoA (angle of arrival) data because it require more expensive antenna arrays. They also do not have the capability to collect ToA (time of arrival) data because it requires the transmission of a wide-band known sequence [35], which is impossible in the case of localizing (blind) intruders. Spectrum sensing platforms serve as the foundation of the spectrum applications, and transmitter localization is one of the main applications. Other applications include signal classification [36], spectrum anomaly detection [37], sensor selection [38,39], spectral occupancy estimation [40], etc.

Transmitter localization. Localization of an intruder in a field using sensor observations has been widely studied, but most of the works have focused on localization of a single intruder [41,42]. In general, to localize multiple intruders, the main challenge comes from the need to "separate" powers at the sensors [43], i.e., to divide the total received power into power received from individual intruders. Blind source separation is a very challenging problem; only very limited settings allow for known techniques using sophisticated receivers [37,44]. We note that (indoor) localization of a device [13] based on signals received from multiple reference points (e.g., WiFi access points) is a quite different problem (see [45] for a recent survey), as the signals from reference points remain separate, and localization or tracking of multiple devices can be done independently. Recent works on multi-target localization/tracking such as [46] are different in the way that targets are passive, instead of active transmitters in the MTL problem. Among other related works, [47] addresses the challenge of handling time-skewed sensors observations in the MTL problem.

Wireless localization techniques mainly fall into two categories: geometry mapping and fingerprinting-based. Geometry mapping mainly has two subcategories: ranging-based such as trilateration (via RSS/RSSI, ToA, TDoA) and direction-based such as triangulation (via AoA). Fingerprinting-based methods can use all signal physical measurements including but not

limited to amplitude, RSS/RSSI, ToA, TDoA, and AoA. Whenever deep learning is used for localization, it can be considered as a fingerprinting-based method, since it requires a training phase to survey the area of interest and a testing phase to search for (predict) the most likely location.

Deep learning for wireless localization. Quite a few recent works have harnessed the power of deep learning in the general topic of localization. E.g., DeepFi in [48] designs a restricted Bolzmann machine that localizes a single target using WiFi CSI amplitude data. DLoc in [9] uses WiFi CSI data as well. Its novelty is to transform CSI data into an image and then uses an image-to-image translation method to localize a single target. MonoDCell in [49] designs an LSTM that localizes a single target in indoor environment using cellular RSS data. [35] designs a three-layer neural network that locations a single transmitter. `DeepTxFinder` in [7] uses CNN to address the same `MTL` problem using RSS data in this paper.

Transmitter Power Estimation. There are several works that estimate the transmission power of a single transmitter. [28] studies the "blind" estimation of transmission power based on received-power measurements at multiple cooperative sensor nodes using maximum likelihood estimation. Blind means there is no prior knowledge of the location of the transmitter or transmit power. [27] propose an iterative technique that jointly estimate the location and power of a single primary transmitter. In [29], the primary transmitter location and power is jointly estimated by a constrained optimization method. [6] uses the maximum likelihood estimation method to estimate the power of an isolated single transmitter and adopts an online learning method to estimate the power of multiple close by transmitters simultaneously.

9. Conclusion

In this paper, we have designed and developed some novel deep learning based scheme (`DeepMTL`) for the multiple transmitter localization (`MTL`) problem. We extended this problem to localizing the intruders in the presence of authorized users and developed a novel technique to solve it. We also developed a novel technique that can solve the multiple transmitter power estimation (`MTPE`) problem. Solving the general MTL and MTPE are both achieved by utilizing our robust `DeepMTL` as a building block. We evaluated all our methods extensively through data simulated from two propagation models as well as a small-scale data collected from a real world testbed. Our developed technique outperforms prior approaches by a significant margin in all performance metrics.

Declaration of competing interest

The authors declare that they have no known competing financial interests or personal relationships that could have appeared to influence the work reported in this paper.

Acknowledgments

References

[1] J.G. Andrews, et al., What will 5G be? IEEE J. Sel. Areas Commun. (2014).
[2] A. Narayanan, X. Zhang, et al., A variegated look at 5G in the wild: Performance, power, and QoE implications, in: ACM SIGCOMM, 2021.
[3] Electromagnetic Spectrum Superiority Strategy, Tech. rep., US Department of Defence, 2020.
[4] H. Kour, R.K. Jha, S. Jain, A comprehensive survey on spectrum sharing: Architecture, energy efficiency and security issues, J. Netw. Comput. Appl. (2018).
[5] M. Khaledi, et al., Simultaneous power-based localization of transmitters for crowdsourced spectrum monitoring, in: MobiCom, ACM, 2017.
[6] C. Zhan, H. Gupta, A. Bhattacharya, M. Ghaderibaneh, Efficient localization of multiple intruders for shared spectrum system, in: IPSN, 2020.
[7] A. Zubow, S. Bayhan, P. Gawłowicz, F. Dressler, DeepTxFinder: Multiple transmitter localization by deep learning in crowdsourced spectrum sensing, in: ICCCN, 2020.
[8] A. Chakraborty, M.S. Rahman, H. Gupta, S.R. Das, Specsense: Crowdsensing for efficient querying of spectrum occupancy, in: INFOCOM, 2017.
[9] R. Ayyalasomayajula, A. Arun, et al., Deep learning based wireless localization for indoor navigation, in: MobiCom, 2020.
[10] C. Zhan, M. Ghaderibaneh, P. Sahu, H. Gupta, DeepMTL: Deep learning based multiple transmitter localization, in: IEEE 22nd International Symposium on a World of Wireless, Mobile and Multimedia Networks (WoWMoM), 2021.
[11] C.W. Kim, et al., Design and implementation of an end-to-end architecture for 3.5 GHz shared spectrum, in: IEEE DySPAN, 2015.
[12] L. Hartung, M. Milind, Policy driven multi-band spectrum aggregation for ultra-broadband wireless networks, in: DySPAN, 2015.
[13] P. Bahl, V.N. Padmanabhan, RADAR: An in-building RF-based user location and tracking system, in: IEEE INFOCOM, 2000.
[14] J. Redmon, et al., YOLOv3: An incremental improvement, 2018, CoRR.
[15] J.D. Hunter, Matplotlib: A 2D graphics environment. https://matplotlib.org/stable/api/_as_gen/matplotlib.pyplot.psd.html.
[16] O. Ronneberger, P. Fischer, T. Brox, UNet: Convolutional networks for biomedical image segmentation, in: MICCAI 2015, 2015.
[17] W. Luo, Y. Li, R. Urtasun, R.S. Zemel, Understanding the effective receptive field in deep convolutional neural networks, 2017, CoRR.
[18] Y. Wu, K. He, Group normalization, 2018, CoRR URL http://arxiv.org/abs/1803.08494.
[19] S. Ioffe, C. Szegedy, Batch normalization: Accelerating deep network training by reducing internal covariate shift, 2015, CoRR.
[20] D.P. Kingma, J. Ba, Adam: A method for stochastic optimization, 2017.
[21] L. Liu, W. Ouyang, X. Wang, P.W. Fieguth, J. Chen, X. Liu, M. Pietikäinen, Deep learning for generic object detection: A survey, 2018, CoRR arXiv:1809.02165.

[22] B. Alizadeh Kharazi, A.H. Behzadan, Flood depth mapping in street photos with image processing and deep neural networks, Comput. Environ. Urban Syst. (2021).

[23] J. Redmon, S. Divvala, R. Girshick, A. Farhadi, You only look once: Unified, real-time object detection, in: CVPR, 2016.

[24] R. Girshick, et al., Rich feature hierarchies for accurate object detection and semantic segmentation, in: CVPR, 2014.

[25] E. Linder-Norén, Open source YOLOv3 implementation, 2019, URL https://github.com/eriklindernoren/PyTorch-YOLOv3.

[26] T. Lin, M. Maire, S.J. Belongie, L.D. Bourdev, R.B. Girshick, et al., Microsoft COCO: common objects in context, 2014.

[27] O. Üreten, T.J. Willink, Joint estimation of emitter power and location in cognitive radio networks, in: 2011 IEEE 12th International Workshop on Signal Processing Advances in Wireless Communications, 2011, pp. 61–65.

[28] M. Zafer, B.J. Ko, I.W.-H. Ho, Transmit power estimation using spatially diverse measurements under wireless fading, IEEE/ACM Trans. Netw. 18 (2010).

[29] S. Kim, H. Jeon, H. Lee, J. Ma, Robust transmission power and position estimation in cognitive radio, 2007.

[30] F. Pedregosa, G. Varoquaux, et al., Scikit-learn: Machine learning in python, J. Mach. Learn. Res. (2011).

[31] J.A. Magliacane, SPLAT! A terrestrial RF path analysis application for Linux/Unix. Downloaded at https://www.qsl.net/kd2bd/splat.html.

[32] K. Chamberlin, et al., An evaluation of longley-rice and GTD propagation models, IEEE Trans. Antennas and Propagation (1982).

[33] S. Rajendran, R. Calvo-Palomino, D. Giustiniano, et al., Electrosense: Open and big spectrum data, IEEE Commun. Mag. (2018).

[34] B. Reynders, F. Minucci, E. Perenda, et al., SkySense: Terrestrial and aerial spectrum use analysed using lightweight sensing technology with weather balloons, in: MobiSys, 2020.

[35] I.B.F. de Almeida, M. Chafii, A. Nimr, G. Fettweis, Blind transmitter localization in wireless sensor networks: A deep learning approach, in: IEEE PIMRC, 2021.

[36] S. Rajendran, et al., Deep learning models for wireless signal classification with distributed low-cost spectrum sensors, IEEE TOCCN (2018).

[37] Z. Li, Z. Xiao, B. Wang, B.Y. Zhao, et al., Scaling deep learning models for spectrum anomaly detection, in: MobiHoc, ACM, 2019.

[38] A. Bhattacharya, C. Zhan, A. Maji, H. Gupta, S.R. Das, P.M. Djurić, Selection of sensors for efficient transmitter localization, IEEE/ACM Trans. Netw. (2021).

[39] A. Bhattacharya, M. Abhishek, J.P. Champati, J. Gross, et al., Fast and efficient online selection of sensors for transmitter localization, in: International Conference on COMmunication Systems & NETworkS, 2022.

[40] S. Sarkar, M. Buddhikot, A. Baset, S.K. Kasera, DeepRadar: A Deep-Learning-Based Environmental Sensing Capability Sensor Design for CBRS, in: MobiCom, 2021.

[41] A. Chakraborty, A. Bhattacharya, S. Kamal, S.R. Das, H. Gupta, P.M. Djuric, Spectrum patrolling with crowdsourced spectrum sensors, in: IEEE Infocom, 2018.

[42] A. Dutta, M. Chiang, "See Something, Say Something" crowdsourced enforcement of spectrum policies, IEEE TOWC (2016).

[43] N. Patwari, et al., Locating the nodes: cooperative localization in wireless sensor networks, IEEE Signal Process. Mag. (2005).

[44] M. Schmidt, et al., Wireless interference identification with convolutional neural networks, in: INDIN, 2017.

[45] F. Zafari, A. Gkelias, et al., A survey of indoor localization systems and technologies, IEEE Commun. Surv. Tutor. (2019).

[46] C. Karanam, et al., Tracking from one side – multi-person passive tracking with wifi magnitude measurements, in: ACM/IEEE IPSN, 2019.

[47] M. Ghaderibaneh, M. Dasari, H. Gupta, Multiple transmitter localization under time-skewed observations, in: DySPAN, 2019.

[48] X. Wang, L. Gao, S. Mao, S. Pandey, Csi-based fingerprinting for indoor localization: A deep learning approach, IEEE Trans. Veh. Technol. (2017).

[49] H. Rizk, et al., MonoDCell: A ubiquitous and low-overhead deep learning-based indoor localization with limited cellular information, in: SIGSPATIAL, 2019.